Visible Light Photocatalysis with Platinized Rutile TiO_2 for Aqueous Organic Oxidation

Bo Sun,† Panagiotis G. Smirniotis,*,† and P. Boolchand‡

Department of Chemical and Materials Engineering, and Department of Electrical & Computer Engineering and Computer Science, University of Cincinnati, Cincinnati, Ohio 45221

Received May 11, 2005. In Final Form: September 15, 2005

Platinized rutile TiO_2 samples containing varying concentrations of Pt were synthesized using Kemira (KE, BET surface area 50 m^2/g, from Finland), and Toto HT0270 (HT, BET surface area 2.9 m^2/g, from Japan) as the starting materials by solution mixing followed by sintering the precursors. Photocatalytic activities were established for phenol oxidation under visible light (wavelength >400 nm). Our results show optimal performance for 8 wt % platinized KE (8 wt % Pt/KE) and $^1/_2$ wt % platinized HT rutile samples. The specific roles of O_2 and visible light were examined using the 8 wt % Pt/KE sample in either N_2 gas ambient or no illumination. Separately, 8 wt % platinized SiO_2 was tested to compare its performance with that of platinized rutile TiO_2. Several other chemicals containing different functional groups (formic acid, salicylic acid, 4-chlorophenol, 2,4,6-trichlorophenol, diethyl phosphoramidate) were selected for photooxidation tests with $^1/_2$ wt % platinized HT rutile. X-ray diffraction reveals Pt metal clusters segregating on the surface of rutile TiO_2 particles with increasing Pt weight percent. The Pt cluster surface area broadly increases, while the effective optical band gap steadily decreases with platinization of the rutile samples. These results suggest that Pt clusters on the surface of rutile TiO_2 particles serve to mediate electron transfer from rutile to O_2, thus facilitating photooxidation of organic chemicals.

Introduction

TiO_2 is one of the most popular semiconductors for photooxidation of organic compounds present in air and water as part of a large-scale remediation of the environment. TiO_2 exists mainly in two polymorphs,[1,2] anatase and rutile. Most studies have focused on anatase and Degussa P25[3−5] TiO_2 (a mixture of anatase and rutile with a ratio of 3∼4:1, nonporous, 50 m^2/g) due to their high photocatalytic activities. Anatase has a band gap of 3.2 eV or a band edge at a wavelength (λ) of 387 nm close to UV radiation. Since UV occupies only about 4% of the solar spectrum, the need to develop photocatalysts with smaller band gaps is paramount.[6−12] Rutile has a slightly smaller band gap of 3.0 eV or a band edge at $\lambda = 413$ nm. But rutile is believed to be much less active in relation to anatase as a photocatalyst.[1,2]

Oxygen is crucial for photooxidation of organic compounds.[2,13−16] From studies on the (110) surface of rutile, Lu et al.[17] have determined that oxygen cannot be adsorbed on a defect-free rutile surface. The O_2 hopping rate depends on the number of oxygen vacancies in TiO_2, and the latter also determines the density of conduction electrons.[18] Thus, electrons created in the interior of a rutile particle following light absorption cannot be efficiently transferred to surface O_2 due to an insufficient concentration of active oxygen vacancies on particle surfaces. The result is a high electron−hole recombination rate, thus limiting[2,19−21] the activity of rutile for organic photooxidation.[2,22]

Deposition of noble metal such as Pd,[23] Pt,[24−26] Au,[27−29] and Ag[30,31] on anatase and Degussa P25 TiO_2 has been

* Corresponding author. Phone: 1-513-556-1474. Fax: 1-513-556-3473. E-mail: Panagiotis.Smirniotis@uc.edu.

† Department of Chemical and Materials Engineering.

‡ Department of ECECS.

(1) Hoffmann, M. R.; Martin, S. T.; Choi, W. Y.; Bahnemann, D. W. *Chem. Rev.* **1995**, *95*, 69.

(2) Fox, M. A.; Dulay, M. T. *Chem. Rev.* **1993**, *93*, 341.

(3) Nargiello, M.; Herz, T. *Photocatalytic Purification and Treatment of Water and Air*; Ollis, D. F., Al-Ekabi, H., Eds.; Elsevier: Amsterdam; New York, 1993; pp 801−807.

(4) Stylidi, M.; Kondarides, D. I.; Verykios, X. E. *Appl. Catal., B* **2003**, *40*, 271.

(5) Anpo, M.; Takeuchi, M. *J. Catal.* **2003**, *216*, 505.

(6) Bach, U.; Lupo, D.; Comte, P.; Moser, J. E.; Weissortel, F.; Salbeck, J.; Spreitzer, H.; Gratzel, M. *Nature* **1998**, *395*, 583.

(7) Gratzel, M. *Nature* **2003**, *421*, 586.

(8) Khan, S. U. M.; Al-Shahry, M.; Ingler, W. B. *Science* **2002**, *297*, 2243.

(9) Zou, Z. G.; Ye, J. H.; Sayama, K.; Arakawa, H. *Nature* **2001**, *414*, 625.

(10) Asahi, R.; Morikawa, T.; Ohwaki, T.; Aoki, K.; Taga, Y. *Science* **2001**, *293*, 269.

(11) Sun, B.; Reddy, E. P.; Smirniotis, P. G. *Appl. Catal., B* **2005**, *57*, 139.

(12) Davydov, L.; Reddy, E. P.; France, P.; Smirniotis, P. G. *J. Catal.* **2001**, *203*, 157.

(13) Wong, J. C. S.; Linsebigler, A.; Lu, G.; Fan, J.; Yates, J. T. *J. Phys. Chem.* **1995**, *99*, 335.

(14) Gerischer, H.; Heller, A. *J. Phys. Chem.* **1991**, *95*, 5261.

(15) Schwitzgebel, J.; Ekerdt, J. J.; Gerischer, H.; Heller, A. *J. Phys. Chem.* **1995**, *99*, 5633.

(16) Gerischer, H.; Heller, A. *J. Electrochem. Soc.* **1992**, *139*, 113.

(17) Lu, G. Q.; Linsebigler, A.; Yates, J. T. *J. Chem. Phys.* **1995**, *102*, 3005; Linsebigler, A.; Lu, G. Q.; Yates, J. T. **1995**, *103*, 9438.

(18) Wahlstom, E.; Vestergaard, E. K.; Schaub, R.; Ronnau, A.; Vestergaard, M.; Laegsgaard, E.; Stensgaard, I.; Besenbacher, F. *Science* **2004**, *303*, 511.

(19) Turchi, C. S.; Ollis, D. F. *J. Catal.* **1990**, *122*, 178.

(20) Davydov, L.; Smirniotis, P. G. *J. Catal.* **2000**, *191*, 105.

(21) Kormann, C.; Bahmemann, D. W.; Hoffmann, M. R. *Environ. Sci. Technol.* **1991**, *25*, 494.

(22) Serpone, N.; Pelizzetti, E. *Photocatalysis: Fundamentals and Applications*; Wiley-Interscience: New York, 1989; pp 78−121.

(23) Wang, C. M.; Heller, A.; Gerischer, H. *J. Am. Chem. Soc.* **1992**, *114*, 5230.

(24) Jaffrezicrenault, N.; Pichat, P.; Foissy, A.; Mercier, R. *J. Phys. Chem.* **1986**, *90*, 2733.

(25) Sun, B.; Vorontsov, A. V.; Smirniotis, P. G. *Langmuir* **2003**, *19*, 3151.

(26) Ohtani, B.; Iwai, K.; Nishimoto, S.; Sato, S. *J. Phys. Chem. B* **1997**, *101*, 3349

(27) Dobosz, A.; Sobczynski, A. *Monatsh. Chem.* **2001**, *132*, 1037.

(28) Subramanian, V.; Wolf, E. E.; Kamat, P. V. *J. Am. Chem. Soc.* **2004**, *126*, 4943.

(29) Subramanian, V.; Wolf, E. E.; Kamat, P. V. *Langmuir* **2003**, *19*, 469.

(30) Crittenden, J. C.; Liu, J. B.; Hand, D. W.; Perram, D. L. *Water Res.* **1997**, *31*, 429.

(31) Scalfani, A.; Mozzanega, M. N.; Herrmann, J. M. *J. Catal.* **1997**, *168*, 117.

10.1021/la051262n CCC: $30.25
Published on Web 10/28/2005

Table 1. Characteristics of the Kemira and HT0270 Rutile TiO_2 Particles in the Starting Materials

catalyst	BET surface area m^2/g[a]	TiO_2 %[b]	form[c]	primary particle size nm[d]
KE	52	89	rutile	25
HT0270	2.9	>99.99	rutile	450

[a] Measured on the Gemini instrument (Micromeritics) at 77 K. [b] Table S_1 in the Supporting Information. [c] Characterized by XRD (Figure 1). [d] Equivalent diameter calculated with the BET surface area.

attempted in the past to increase their photoefficiencies by increasing the rate of electron transfer from TiO_2 to O_2.[16,32] In this study, we have attempted to modify the surface of rutile TiO_2 particles by depositing platinum nanoclusters and have examined the photocatalytic performance of these platinized rutile particles. The photoactivities of both pristine (with no Pt) and platinized rutile were measured. Our results show platinized rutile to be far more active than pristine rutile. A possible interpretation for the observation is advanced.

Experimental Section

Catalyst Synthesis. The starting materials included commercial rutile titania powders, Kemira (KE, BET surface area 50 m^2/g) from Finland and Toto HT0270 (HT, BET surface area 2.9 m^2/g) from Japan. Their characteristics are summarized in Table 1. KE samples containing Pt weight percentages of 1, 4, 6, 8, 10, and 14 were synthesized. HT samples containing Pt weight percentages of $^1/_8$, $^1/_4$, $^1/_2$, 1, 2, 4, 6, and 8 were also synthesized. In a typical Pt loading, $^1/_4$ g of dry rutile powder was mixed with certain amounts of H_2PtCl_6 solution containing $^1/_4$ wt % of Pt. Then distilled water was added to result in a 20 mL volume as described elsewhere.[25] The mixture was slowly stirred for 20 min. The slurry was then heated to 70 °C with vigorous stirring until dry. The dry powder was then oxidized in a quartz reactor using ultrahigh-purity oxygen (from Matheson). The final step was a reduction of the powder at 380 °C for 2 h using ultrahigh-purity hydrogen (from Matheson). Separately, 8 wt % Pt-deposited silica was synthesized using the same method with 40% Ludox HS-40 colloidal silica (Aldrich) as the silica source.

X-ray Diffraction (XRD). The pristine and platinized rutile samples were examined in powder XRD to establish the nature of the crystalline phases present. A Nicolet powder X-ray diffractometer equipped with a Cu Kα source (wavelength = 0.154 nm) was used to excite the Bragg scattering and 2θ scans in the 20−50° range were recorded as shown in Figure 1. Scans of platinum black powder (Matheson Coleman & Bell, PX1266) were also recorded for reference.

Surface Area of Pt/Rutile Catalysts and Pt Surface Area Measurements. The BET surface area of the catalysts was measured on a Gemini instrument (Micromeritics) at 77 K using liquid nitrogen. The platinum surface area and metal dispersion of the samples were measured using H_2 chemisorption on an Autochem 2910 instrument from Micromeritics at 50 °C. Prior to the experiment, the catalysts were pretreated with pure H_2 at 370 °C for 2 h. It was assumed that one H atom is absorbed on one Pt atom. The inferred Pt surface area as a function of Pt weight percent in the samples are plotted in Figures 2 and 3.

Optical Band Gap. A UV−VIS spectrophotometer (Shimadzu 2501PC) with an integrating sphere attachment ISR1200 for diffuse reflectance measurements was used to establish the optical band gap of the pristine and platinized rutile samples. The optical absorption was measured in the 200−900 nm range. The optical edge or gap was inferred by linear extrapolation of the absorbance from the high-slope region (Figures 4 and 5). $BaSO_4$ was used as the standard for these measurements.

Transmission Electron Microscopy (TEM). Structures of some platinized rutile TiO_2 samples were investigated on a Philips CM20 microscope (LaB_6 cathode, operated at 200 kV). A sample was deposited onto a copper grid after it was dispersed in methanol by an ultrasonic bath. Typical TEM scans of the samples are shown in Figure 6a−c.

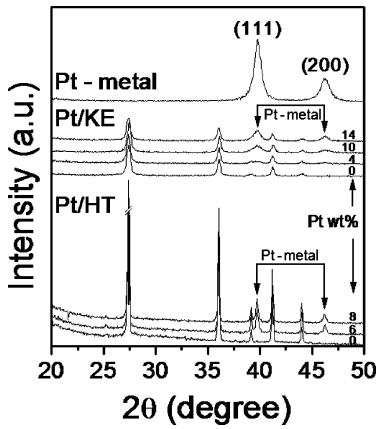

Figure 1. XRD of Pt metal powder, Pt/KE, and Pt/HT rutile samples. Note that in both rutile samples, Pt metal inclusions occur as suggested by the observed (111) and (200) Bragg peaks. Furthermore, since the particle size of KE rutile is much smaller than that of HT, line widths of the Bragg reflections in the former samples are broader than those in the latter samples.

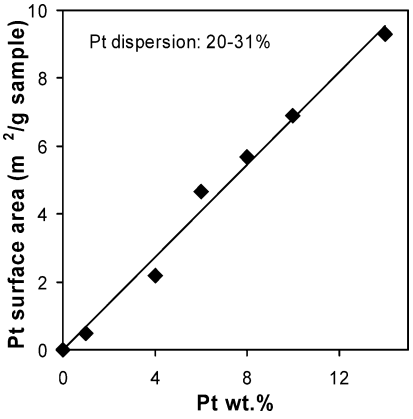

Figure 2. Linear increase in Pt surface area of KE rutile samples as a function of Pt wt %. The increase suggests that Pt metal clusters dress the surface of rutile particles.

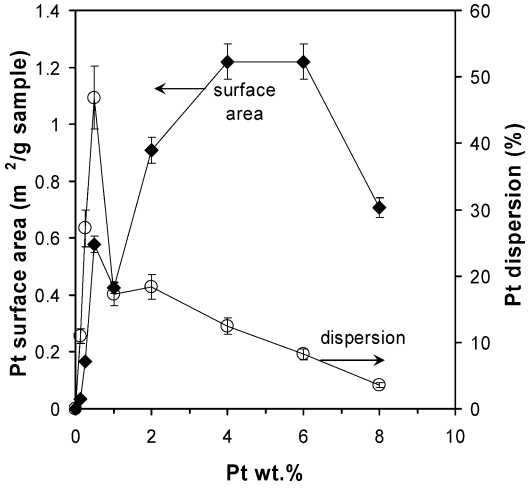

Figure 3. Pt dispersion (○) and surface area (◆) of HT rutile samples as a function of Pt wt %.

Photocatalytic Activity of Platinized Rutile Samples. A batch round flat-plate reactor[11,12] was used to test activities of synthesized samples for phenol degradation under visible light. Water (18.0 MΩ·cm, NANOPURE ultrapure water system, Barnsted/Thermolyne, model no. D4754) was used in all the tests. The reaction suspension consisted of 500 mL of 1 mM phenol and 0.2 g/l platinized rutile TiO_2. The irradiation source was a 450

(32) Linsebigler, A.; Lu, G. Q.; Yates, J. T. *Chem. Rev.* **1995**, *95*, 735.

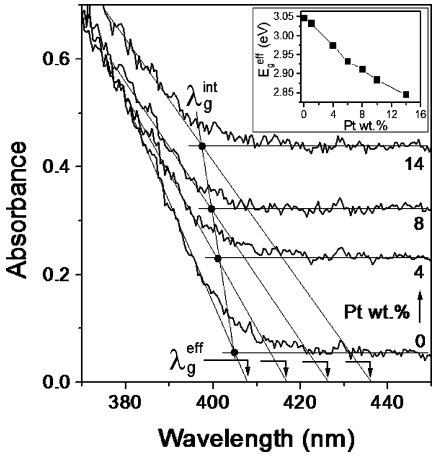

Figure 4. Optical absorption tails observed in KE rutile samples showing a red shift with increasing Pt weight percent. The linearly extrapolated wavelength, λ_g^{eff}, corresponding to vanishing absorbance, is taken as a measure of the effective optical gap $E_g^{eff}(\text{eV}) = 1239.6/\lambda_g^{eff}(\text{nm})$. The inset reveals the steadily decreasing E_g^{eff} with Pt wt %. The intrinsic band gap of Pt/rutile, on the other hand, is found to mildly increase, i.e., λ_g^{int} shifts to a smaller wavelength with increasing Pt content as shown by the filled circles (●). Here, λ_g^{int} represents the intercept of the absorption with the flat background.

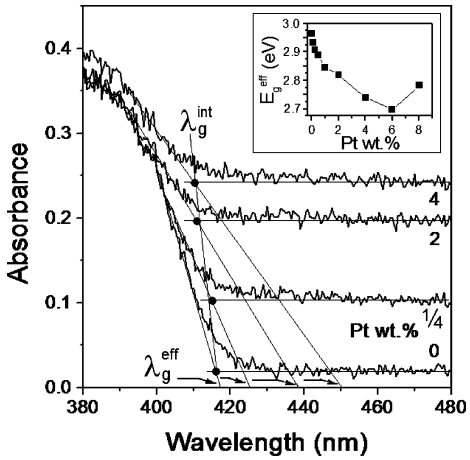

Figure 5. Optical absorption tails observed in HT rutile samples showing a red shift with increasing Pt weight percent. The linearly extrapolated wavelength, λ_g^{eff}, corresponding to vanishing absorbance, is taken as a measure of the effective optical gap $E_g^{eff}(\text{eV}) = 1239.6/\lambda_g^{eff}(\text{nm})$. The inset reveals the steadily decreasing E_g^{eff} with Pt wt % (<6%). The intrinsic band gap of Pt/rutile, on the other hand, is found to mildly increase, i.e., λ_g^{int} shifts to a smaller wavelength with increasing Pt content as shown by the filled circles (●).

Watts medium-pressure mercury lamp (Jelight, J05PM1HGC2). A double acrylic OP-2 (museum quality) sheet was placed between the light source and the reactor for the purpose of absorbing UV radiation (λ < 400 nm). A cooling jacket around the reactor allowed the IR part of the light spectrum to be absorbed and precluded heating of the reaction solution. The light power density on the sheet was measured at 70 μW/cm^2 in our setup by using a radiometer detector system (International Light, Inc., model IL 1700, and SED033 no. 3435). The reaction temperature was kept at 25.0 ± 0.5 °C. The pH of the reaction suspension was not adjusted. The suspended catalyst in an aqueous system was oxygenated (Wright Brothers, 99.9% oxygen gas) at 0.5 L/min to ensure complete saturation. The reaction suspension samples were taken with a syringe at different time intervals and filtered with Cameo 25P polypropylene syringe filters (OSMONICS, cat. no. DDP02T2550). Sample solutions were analyzed with a total organic carbon analyzer (TOC-VCSH, Shimadzu) and scanned on the UV−VIS spectrophotometer (Shimadzu 2501PC). Figures 7 and 8 provide results on photooxidation of phenol. Three

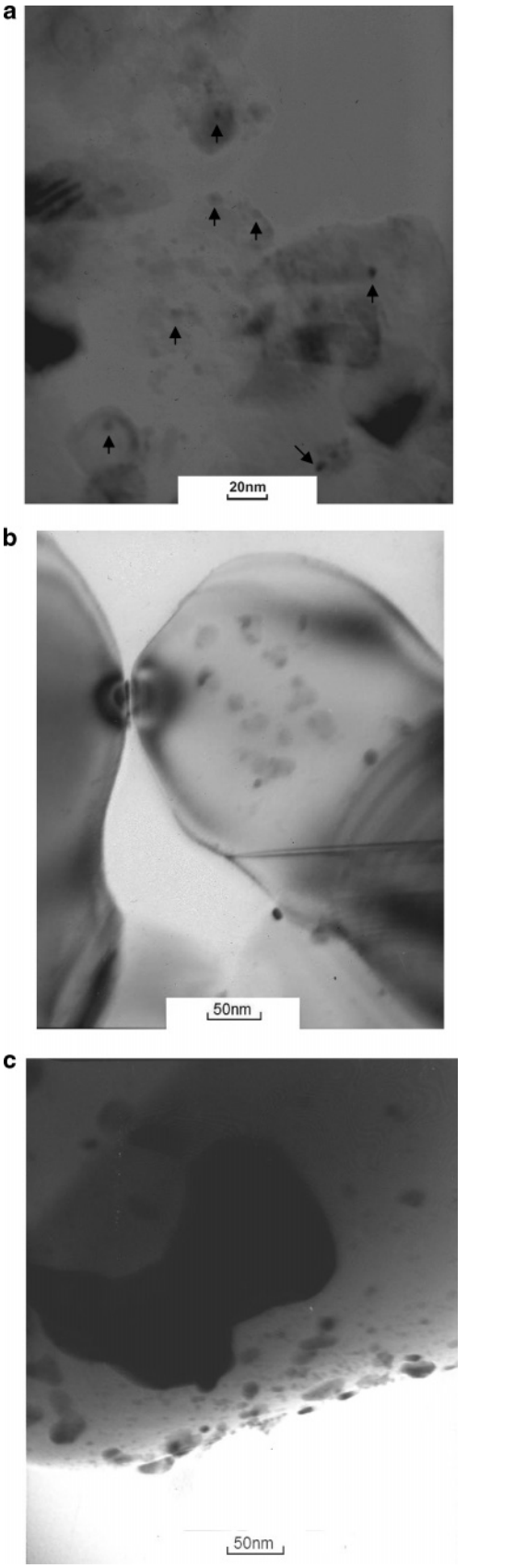

Figure 6. (a) TEM of 8 wt % Pt/KE. The small black dots (~5 nm) with arrows represent Pt inclusions. The large chunks (~30 nm) represent KE TiO_2 particles. (b) TEM of 1/2 wt % Pt/HT showing Pt inclusions as small black dots (~25 nm). The large chunks (~500 nm) represent HT TiO_2 particles. (c) TEM of 6 wt % Pt/HT. The small black dots (~30 nm) represent Pt inclusions and the big black region (~200 nm) represents a large Pt aggregate.

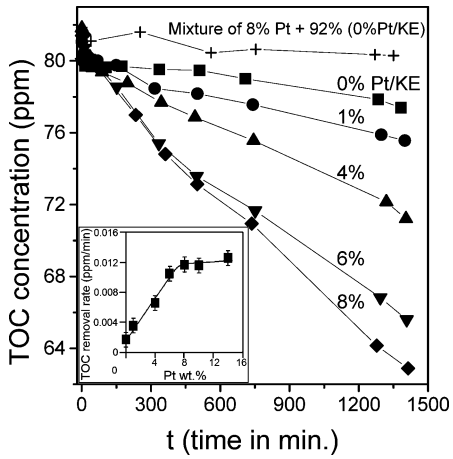

Figure 7. Total organic carbon (TOC) concentration with increasing time during phenol photooxidation under visible light using Pt/KE. Catalyst concentration, 0.2 g/L; initial phenol concentration, 1 mM; temperature, 25 ± 0.5 °C. The inset shows the relation of TOC removal rate with respect to Pt wt % in Kemira rutile. The TOC removal rate is equal to the slope of the corresponding curve.

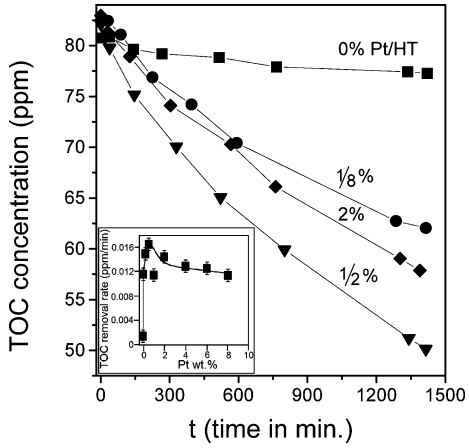

Figure 8. Total organic carbon (TOC) concentration with increasing time during phenol photooxidation under visible light using Pt/HT. Catalyst concentration, 0.2 g/L; initial phenol concentration, 1 mM; temperature, 25 ± 0.5 °C. The inset shows the relation of TOC removal rate with respect to the percentage of Pt deposited on HT rutile TiO_2. The TOC removal rate is obtained by linear correlation of the part of the corresponding curve after 500 min of reaction.

Table 2. Conditions of the Three Comparison Experiments

no.	catalyst (0.2 g/L)	gas passing through the suspension (0.5 L/min)	light
1	8 wt % Pt/SiO_2	O_2	vis light
2	8 wt % Pt/KE TiO_2	O_2	dark
3	8 wt % Pt/KE TiO_2	N_2	vis light

comparison studies (Table 2) were undertaken to understand the role of rutile TiO_2, visible light, and O_2 in the photocatalytic organic oxidation. The corresponding results are shown in Figure 9 with those of 8% Pt/KE and $^1/_2$% Pt/HT under visible light with O_2 passing through.

The most active photocatalyst ($^1/_2$ wt % Pt/HT) found for phenol photooxidation was also tested with salicylic acid (SA, 1 mM), diethylphosphoramidate (DEPA, 1.5 mM), 4-chlorophenol (4-CP, 1 mM), 2,4,6-chlorophenol (2,4,6-CP, 1 mM), and formic acid (6 mM) as probe molecules. The samples were taken and measured in the same way as above. The results are presented in Figure 10.

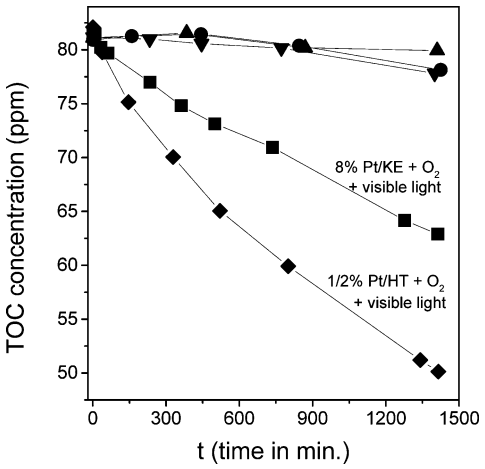

Figure 9. Total organic carbon (TOC) concentration with increasing time during phenol photooxidation with the conditions specified in Table 2: ● represents 8% Pt/SiO_2 + O_2 + visible light; ▲ represents 8% Pt/KE + O_2 + dark; ▼ represents 8% Pt/KE + N_2 + visible light. The performances of 8 wt % Pt/KE (Figure 7) and $^1/_2$ wt % Pt/HT (Figure 8) with O_2 passing through under visible light are also shown for comparison. Catalyst concentration, 0.2 g/L; initial concentrations of phenol, 1 mM; temperature: 25 ± 0.5 °C.

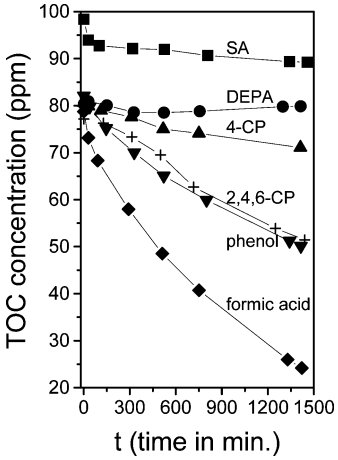

Figure 10. Total organic carbon (TOC) concentration with increasing time during photooxidation of organic chemicals under visible light using $^1/_2$ wt % Pt/HT catalyst. Catalyst concentration, 0.2 g/L; initial concentrations of organic chemicals, DEPA (1.5 mM), salicylic acid (1 mM), 4-chlorophenol (1 mM), phenol (1 mM), formic acid (6 mM); temperature: 25 ± 0.5 °C.

Results and Discussion

Our XRD scans (Figure 1) of platinized KE and HT samples show reflections characteristic of the rutile phase but no reflections of the anatase phase.[33] Furthermore, reflections characteristic of the rutile phase do not shift measurably upon platinization. On the other hand, with increasing Pt weight percent we observe (111) and (200) reflections of Pt metal near 39.8° and 46.3° to steadily increase in intensity for both the KE and HT samples. The result suggests that the Pt additive largely segregates in the elemental form. These reflections are measurably broad for the KE samples, and from the observed full width at half-maximum (Figure 1) and the Scherrer formula,[34] we deduce a size of 11 ± 2 nm (Table 3) for the Pt metal clusters on KE.

(33) Sun, B.; Smirniotis, P. G. *Catal. Today* **2003**, *88*, 49.
(34) Kakudo, M. *X-ray Diffraction by Polymers*; Elsevier: Tokyo, Kodansha, Amsterdam, New York, 1972; p 239.

Table 3. Pt Metal Cluster Size on the Surface of KE and HT Rutile Particles Established from XRD Measurements[a]

Pt/KE						Pt/HT		
Pt (%)	4	6	8	10	14	Pt (%)	6	8
Pt particle size (nm)[b]	11	10	11	10	13	Pt particle size (nm)[b]	29	28

[a] Note that the particle size of the HT/rutile is much larger than that of KE/rutile (Table 1). [b] The Pt particle size, t, in XRD measurements, is inferred from the Scherrer formula (ref 19), $t = 0.94\lambda/(\beta \cos \theta)$, where λ is the wavelength of the X-rays (0.154 nm for a Cu Kα source), β is the observed half-width of the Bragg reflection, and θ is the Bragg peak position.

The BET surface area of the Pt/KE samples is 50 ± 3 m^2/g. The platinum surface area of the Pt/KE samples increases by 0.68 ± 0.03 m^2/(g catalyst) with each percentage of Pt deposited on the KE rutile sample (Figure 2). The Pt particle size estimated from the H_2 chemisorption measurement is around 5 nm. This number is in reasonable agreement with the XRD-inferred size of 11 nm (Table 3). The platinum surface areas and dispersions of the Pt/HT samples are shown in Figure 3. The trend of Pt surface area of Pt/HT is different from that of Pt/KE. The BET surface area of all the Pt/HT samples is 2.5 ± 0.3 m^2/g, which is an order of magnitude lower than that of the KE rutile samples. Thus, the capacity of the HT rutile samples for Pt deposition is much smaller. When the deposited Pt amount is less than $^1/_2$ wt %, the additive disperses well as reflected by the increasing Pt dispersion (Figure 3). However, the behavior rapidly saturates, and a decrease of Pt dispersion occurs upon further Pt deposition on HT (Figure 3). This can be related to the increasing possibility of Pt clusters coalescing on the large-sized HT particle surface. When the deposited Pt weight percent reaches 4%, the Pt surface area increases to 1.2 m^2/g, which is nearly half of the whole TiO_2 surface area (Table 1). The chance for the originally separated Pt islands to coalesce is large, and they tend to agglomerate, thus, decreasing the Pt surface area with further Pt deposition (Figure 3). Although the XRD results alone cannot localize whether the Pt clusters form in the interior or on the surface of the rutile particles, the H_2 chemisorption experiments unambiguously suggest that these clusters form on the surface of the rutile grains.

The band gap of pure KE rutile TiO_2 of 3.05 eV observed here is consistent with previous reports.[35,36] Platinized KE samples display a higher absorbance of light in the visible range (λ > 410 nm) than that of pure rutile TiO_2. The absorbance increases with the amount of Pt because of light scattering, suggesting that the *effective* optical absorption edge shifts to a longer wavelength (Figure 4) as measured by the extrapolated value of λ when the absorbance goes to zero.[37−39] On the other hand, it appears that the intrinsic band gap of rutile increases mildly from 3.06 to 3.12 eV with the Pt content as illustrated in Figure 4.[37] Here we measure the band gap by the intercept of the absorbance with appropriate flat background, as illustrated in Figure 4. The UV−VIS spectra of the Pt/HT samples are shown in Figure 5. The band gap of 0% Pt/HT is 2.96 eV, which is smaller than that of 0% Pt/KE. The difference can be due to the larger size of HT TiO_2 particles.[40] Pt deposition increases the absorption of light in the visible range in these HT samples (Figure 5). The slope near the absorption edge becomes smaller with increasing Pt content up to 6%, which is consistent with the observations with the Pt/KE samples above.

TEM pictures of 8% Pt/KE and $^1/_2$% Pt/HT are shown in Figure 6a and 6b, respectively. The KE particle size is around 30 nm, and the size of Pt on KE is around 5 nm, which is about the same as the H_2 pulse chemisorption results. The HT particle size is around 400 nm, and the size of Pt on HT is around 25 nm. The difference in the Pt particle size may be due to the TiO_2 surface curvature and thus TiO_2 particle size. When 6% Pt is deposited on HT, Pt particles with a size around 200 nm can be observed (Figure 6c). This indicates that with more and more Pt deposited on the TiO_2 surface, the Pt particles tend to aggregate if they are too close to each other. This is the reason that Pt dispersion decreases with Pt content when it is higher than $^1/_2$% (Figure 3). The particle size of Pt clusters in the 6% Pt/HT and the 8% Pt/HT obtained by the Scherrer formula is around 29 nm (Table 3), which indicates that the XRD characterizes all Pt particles on an average.

The total organic carbon (TOC) concentration for phenol photooxidation under visible light (λ > 400 nm) with the Pt/KE samples is shown in Figure 7. The 0% Pt/KE samples display a negligible photocatalytic activity, which is consistent with the literature.[1] O_2 is crucial for photooxidation of organic compounds.[2,13−16] O_2 cannot be adsorbed on the native (defect-free) rutile (110) surface,[17] and the O_2 hopping rate depends on the number of oxygen vacancies.[18] Henderson et al.[41] studied the reaction of O_2 with OH groups adsorbed at defects on rutile (110) and illustrated the electron-scavenging role of O_2 in photocatalysis. The net charge and structure of the Ti^{4+} cation and oxygen ion on the rutile surface[42−46] are different from those on the anatase surface.[35−37,47] Anatase and rutile TiO_2 have different bulk structures and surface energies.[35−37,48] These differences can be the reason for rutile TiO_2's lower capacity to absorb O_2.[2,17] Thus, the O_2 molecule without adsorption can be out of reach of Ti^{3+}, where electrons are trapped on the surface.[1,19] As a result, electrons and holes created inside rutile TiO_2 tend to recombine with each other, giving out heat. Although rutile TiO_2 particles have other surfaces than (110),[49,50] the low activity of 0% Pt/KE indicates a low density of active defect sites for adsorbing O_2 molecules. In order for electrons to be conducted efficiently out from rutile TiO_2

(35) Kavan, L.; Gratzel, M.; Gilbert, S. E.; Klemenz, C.; Scheel, H. J. *J. Am. Chem. Soc.* **1996**, *118*, 6716.
(36) Tang, H.; Prasad, K.; Sanjines, R.; Schmid, P. E.; Levy, F. *J. Appl. Phys.* **1994**, *75*, 2042.
(37) Nakajima, H.; Mori, T.; Watanabe, M. *J. Appl. Phys.* **2004**, *96*, 925.
(38) Li, F. B.; Li, X. Z. *Chemosphere* **2002**, *48*, 1103.
(39) Furube, A.; Asahi, T.; Masuhara, H.; Yamashita, H.; Anpo, M. *Chem. Phys. Lett.* **2001**, *336*, 424.
(40) Hagfeldt, A.; Gratzel, M. *Chem. Rev.* **1995**, *95*, 49.
(41) Henderson, M. A.; Epling, W. S.; Peden, C. H. F.; Perkins, C. L. *J. Phys. Chem. B* **2003**, *107*, 534 and references therein.
(42) Oliver, P. M.; Watson, G. M.; Kelsey, E. T.; Parker, S. C. *J. Mater. Chem.* **1997**, *7*, 563.
(43) Fahmi, A.; Minot, C.; Silvi, B.; Causa, M. *Phys. Rev. B* **1993**, *47*, 11717.
(44) Fahmi, A.; Minot, C. *Surf. Sci.* **1994**, *304*, 343.
(45) Leconte, J.; Markovits, A.; Skalli, M. K.; Minot, C.; Belmajdoub, A. *Surf. Sci.* **2002**, *497*, 194.
(46) Kurtz, R. J.; Stockbauer, R.; Madey, T. E. *Surf. Sci.* **1989**, *218*, 178.
(47) Hadjiivanov, K. I.; Klissurski, D. G. *Chem. Soc. Rev.* **1996**, *25*, 61.
(48) Lazzeri, M.; Vittadini, A.; Selloni, A. *Phys. Rev. B* **2001**, *63*, 155409.
(49) Ohno, T.; Sarukawa, K.; Matsumura, M. *New J. Chem.* **2002**, *26*, 1167.
(50) Diebold, U. *Surf. Sci. Rep.* **2003**, *48*, 53.

to O_2, we dressed the rutile TiO_2 surface with platinum metal.

The photooxidation of organic compounds follows a Langmuir−Hinshelwood rate form.[19] The reaction form is zero-order when the concentration of the reactant compound was high. A catalyst with no deactivation usually photooxidizes organic compounds linear-proportionally with time[19,51] because the amount of active oxygen species for oxidation[1,52] is kept constant during photooxidation. The organic chemical decomposition rate should be proportional to the concentration of oxygen species in solution, which in turn is proportional to the amount of active Pt sites and active defect sites on the TiO_2 surface. This is observed with the Pt/KE samples. The TOC concentration decreases linearly with time during the photocatalytic reaction (Figure 7). The activity increased linearly with the amount of Pt deposition in the range of 0−6 wt % (Figure 7), yielding a slope of 1.4×10^{-3} ppm/min per wt % of Pt. Correspondingly, the rate of electrons transferred per surface Pt atom is 5.3×10^{-4} s^{-1} assuming that one electron is needed for oxidizing one carbon. The increasing activity implies an effective contact between Pt and the KE particles. Trapped electrons on Ti cations can be conducted out through deposited Pt in contact with Ti^{3+}.[53] Oxygen can be adsorbed on Pt surfaces.[54,55] Pt plays the role of bridging trapped electrons to oxygen molecules. Hence, oxygen can be reduced to O_2^-, and in turn the reactive oxygen species form in the aqueous suspension.[19,20] When the Pt percentage is less than 8 wt %, electron transfer through Pt is the limiting step of the reaction. The amount of electrons transferred out of the KE rutile increases with Pt deposition. The particle size of Pt on the KE surface is about 5 nm, that is, one Pt particle covers about 500 TiO_2 unit cells[36] on the surface. A lot of O sites that were originally able to conduct holes out for creation of active oxygen species are smeared and decimated although electrons can be conducted out of Ti atoms at the same time. These factors tend to greatly reduce the catalyst's optimal activity and can be the possible reasons for the activity not increasing any further when Pt deposition is higher than 8 wt %. What is more, the mobility and diffusivity of electrons in rutile are about 2 orders of magnitude lower than those in anatase, which provides more opportunities for the created electrons to recombine with holes in rutile.[25] This can intrinsically limit the activity of rutile. Therefore, the amount of electrons that can be transferred out into O_2 reaches a plateau at 8 wt % Pt deposition on KE rutile.

A simple physical mixture of Pt powder (BET surface area of 18.0 m^2/g) and 0% Pt/KE in the ratio of 8:92 as a catalyst has a negligible photocalytic activity compared to 8 wt % Pt/KE (Figure 7). The result shows that electrons produced in rutile cannot pass to Pt metal without an intimate contact between the Pt and the TiO_2.

To prove further the role of Pt on the rutile TiO_2 surface in conducting the electrons, we examined high-purity HT rutile, which possessed a smaller surface area (Table 1) than KE rutile. Figure 8 shows the TOC concentration curve during phenol photodegradation with Pt/HT samples under visible light. In comparison with the observation with Pt/KE, a decrease of the TOC removal rate with the Pt/HT samples occurs during the first 400 min or so. The 0% Pt/HT sample shows a higher photoactivity than that of 0% Pt/KE. But 0% Pt/HT deactivates during the phenol oxidation, which is not observed in experiments with 0% Pt/KE. This implies that the original active defect sites on the TiO_2 surface are reoxidized by O_2 which moves through the suspension and/or the active sites on other surfaces[50] deactivate little by little. These can also contribute to the observed deactivation with other Pt/HT samples. Furthermore, a change in metal morphology may also contribute to the variation in activity of the nanocomposite catalyst.[56] TOC removal rates become stable after 400 min of reaction, which is attributed to effective integration of Pt and TiO_2. Accordingly, the TOC removal rate with respect to Pt wt % is drawn in Figure 8. The activity of the Pt/HT catalyst first increases with Pt when the Pt deposited is no more than $^1/_2$%, and the activity decreases with further Pt deposition. The initial TOC degradation rate with $^1/_2$% Pt/HT is 0.065 ppm/min, and the final degradation rate is 0.017 ppm/min, which is higher than that with 8% Pt/KE (0.012 ppm/min) although the BET surface area and Pt amount of $^1/_2$% Pt/HT are 1 order of magnitude lower than those of 8% Pt/KE. The rate of electron transfer per surface Pt atom for $^1/_2$ wt % Pt/HT is 7.4×10^{-3} s^{-1}. Therefore, Pt deposited on $^1/_2$% Pt/HT is an order of magnitude more efficient in transferring electrons from rutile to O_2 than that on the 8 wt % Pt/KE sample.

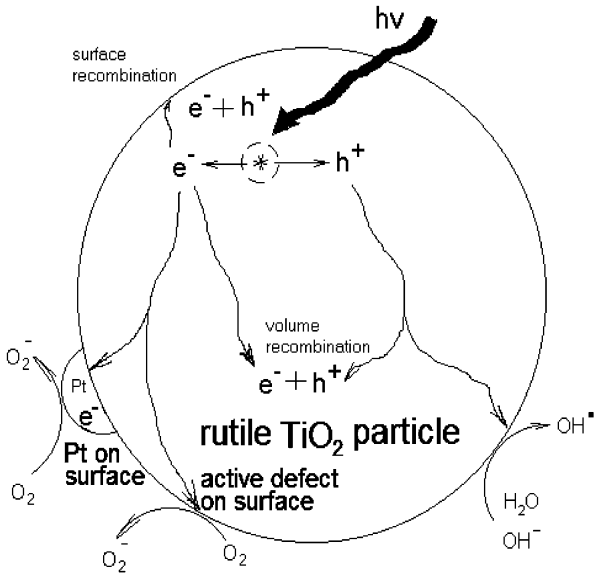

Figure 11. Schematic drawing of the photocatalytic events in Pt/rutile TiO_2 under visible light.

The TOC degradation curves corresponding to the three experiments listed in Table 2 are shown in Figure 9. The phenol degradation during these three comparison tests is found to be negligible compared with that observed with 8% Pt/KE and $^1/_2$% Pt/HT under visible light with O_2 passing. The inactivity of 8 wt % Pt/SiO_2 proves that rutile TiO_2 is needed for the photocatalyst to be active and Pt itself cannot photodegrade phenol efficiently, which is consistent with the result for the 8% Pt (black) and 92% KE physical mixture in Figure 7. The inactivity of 8 wt % Pt/KE in the dark indicates that light is necessary for oxidation. The inactivity of 8 wt % Pt/KE in N_2 instead of O_2 implies the indispensable role of O_2 in accepting electrons and triggering further photocatalytic reactions during organic photooxidation.[1,2]

(51) Okamoto, K.; Yamamoto, Y.; Tanaka, H.; Itaya, A. *Bull. Chem. Soc. Jpn.* **1985**, *58*, 2023.
(52) Matthews, R. W. *Water Res.* **1986**, *20*, 569.
(53) Gan, S.; Liang, Y.; Baer, D. R.; Grant, A. W. *Surf. Sci.* **2001**, *475*, 159.
(54) Mieher, W. D.; Ho, W. *J. Chem. Phys.* **1993**, *99*, 9279.
(55) Zhu, X. Y.; Hatch, S. R.; Campion, A.; White, J. M. *J. Chem. Phys.* **1989**, *91*, 5011.
(56) Cozzoli, P. D.; Fanizza, E.; Comparelli, R.; Curri, M. L.; Agostiano, A.; Laub, D. *J. Phys. Chem. B* **2004**, *108*, 9623.

Figure 10 shows the TOC degradation curves during photooxidation of SA, DEPA, 4-CP, 2,4,6-CP, and formic acid under visible light with the optimal catalyst ($^1/_2$% Pt/HT) obtained above. Among all test molecules, formic acid is the easiest to degrade. In contrast, no removal of DEPA[57] is observed. The degradation rate of 2,4,6-CP is comparable to that of phenol, and both of them are higher than that of 4-CP. The −OH group in the test molecules that can be removed by photocatalysis indicates the importance of organic molecule adsorption on the rutile TiO_2 surface.

With the characterization and discussion above, a mechanism is proposed for photocatalysis with Pt/rutile TiO_2 (see Figure 11). Platinum islands on TiO_2 facilitate efficient transfer of electrons created in rutile TiO_2 to O_2 as active defect sites,[17,18] which initiated further photocatalytic processes.[1,19,20]

Conclusions

Platinized rutile TiO_2 is active for photooxidization of organic chemicals with phenolic and/or acid groups under visible light (λ > 400 nm). Pt, rutile, Pt−rutile contact, O_2, and visible light are necessary elements for efficient organic oxidation. Optimal photocatalytic performances are observed with 8 wt % platinized KE and $^1/_2$ wt % platinized HT rutile samples. The activities of Pt/rutile samples indicate that Pt deposited on rutile TiO_2 can conduct electrons created in rutile out to O_2. Pt deposited on different types of rutile titanias (KE or HT) can have different efficiencies in transferring electrons. The size of the rutile TiO_2 particles can influence the pattern of Pt growth on the TiO_2 particles. The present study shows the intrinsic activity of platinized rutile TiO_2 in aqueous organic photodegradation, which can be useful for environmental cleanup.

Acknowledgment. The authors acknowledge the NSF and the U.S. Department of the Army for partial support for this work through Grants CTS-0097347 and DAAD 19-00-1-0399, respectively. We also acknowledge funding from the Ohio Board of Regents (OBR) that provided matching funds for equipment to the NSF CTS-9619392 Grant through the OBR Action Fund No. 333. The authors thank Udaya K. Vempati in the ECECS department at the University of Cincinnati for assistance in the XRD data collection and analysis.

Supporting Information Available: Ingredients of the Kemira and HT0270 rutile titanias used in the present study (Table S_1); experimental setup for the visible light performance test (Figure S_1); the spectral output of the medium-pressure mercury lamp and transmittance of the Pyrex and acrylic OP-2 filters (Figure S_2). This material is available free of charge via the Internet at http://pubs.acs.org.

LA051262N

(57) Vorontsov, A. V.; Davydov, L.; Reddy, E. P.; Lion, C.; Savinov, E. N.; Smirniotis, P. G. *New J. Chem.* **2002**, *26*, 732.